© Journal for Modeling in Ophthalmology 2022;4:1-18
Review article https://doi.org/10.35119/maio.v4i1.121

From your kidneys to your eyes: lessons from computational kidney models

Melissa M. Stadt[1], Anita T. Layton[1,2]

[1]*Department of Applied Mathematics, University of Waterloo, Waterloo, ON, Canada*, [2]*Department of Biology, Cheriton School of Computer Science, School of Pharmacy, University of Waterloo, Waterloo, ON, Canada*

Abstract

Purpose: The purpose of this review is to describe computational models that have been developed for studying kidney function and how these models may be adapted to study the eyes.
Methods: We derive equations for modeling solute and water transport across epithelial cell membranes in the kidney. These equations describe mass conservation, as well membrane transport via cotransporters, exchangers, and primary active transport.
Results: We describe how computational models of renal transport have been applied to investigate kidney function in physiological and pathophysiological conditions.
Conclusion: The computational models herein described for the kidney may be adapted to study ocular functions and dysfunction.

Keywords: computational model, diabetes, epithelial transport, renal physiology, sex differences

1. Introduction

Like the eyes, the kidneys are organs that are critical to our lives and well-being. Not only do the kidneys function as filters, removing metabolic wastes and toxins from the blood and excreting them through the urine, but they also serve other essential regulatory functions. Through a number of regulatory mechanisms, the kidneys help

Correspondence: Department of Applied Mathematics, University of Waterloo, Waterloo, ON, Canada, N2L 3G1.
E-mail: anita.layton@uwaterloo.ca

maintain the body's water balance, electrolyte balance, and acid-base balance. Additionally, the kidneys produce or activate hormones that are involved in erythrogenesis, calcium metabolism, and the regulation of blood flow and blood pressure.

In humans the kidneys are located in the abdominal cavity, with one kidney on each side of the spine. Each kidney is a bean-like structure that consists of two regions; the outer region is the cortex, and the inner region is the medulla. The cortex contains glomeruli, which are clusters of capillaries, and convoluted segments of tubules, whereas the medulla contains almost parallel arrangement of tubules and vessels. Despite their relatively small size (approximately 0.5% of total body weight), the kidneys receive about 20% of cardiac output. That blood is processed by the functional unit of the kidney, which is the nephron. Each human kidney is populated by approximately a million nephrons; each rat kidney, by approximately 40,000 nephrons. An illustration of a kidney, together with a close-up image of a nephron and its surrounding blood vessels, can be found in Figure 1.

The nephrons maintain water, electrolyte, and acid-base homeostasis by mediating a number of epithelial transport processes. Blood enters the nephron after passing through a filter called the glomerulus. As the filtrate flows along the nephron, the tubular epithelium secretes or reabsorbs water and solutes so that, ultimately, urinary excretion matches daily intake. The kidney adapts to variations in blood volume and composition by modulating the expression and/or activity of its epithelial transporters. These changes are mediated by a variety of hormonal and neuronal signals and involve complex signaling cascades. The heterogeneity of the different nephron segments is crucial for this adaptive capacity. Whereas the proximal tubules reabsorb large amounts of water and solutes iso-osmotically, other tubular epithelia have more specialized functions. In the distal nephron for example, principal cells regulate the reabsorption of sodium and potassium, whereas intercalated cells act mostly to maintain the acid-base balance. A detailed description of the specificities of each segment is beyond the scope of this review. We point the readers to Eaton and Pooler[1] for a more detailed description of the kidneys. We provide here a general framework to represent transepithelial transport at the cellular level. The concept presented for the kidney could potentially be applied to develop a theoretical model of aqueous humor secretion across the ciliary epithelium of the human eye. The clinical implication of such a model would be to predict the value of the intraocular pressure, whose abnormal increase is the established risk factor for glaucoma, the second cause of irreversible blindness worldwide.

2. Modeling solute and water transport across renal tubular epithelia

2.1 Conservation equations

Consider a segment denoted by i, (i = PCT, S3, etc.) at steady state. For a specific cell along the nephron, the cellular, paracellular, and luminal space are represented

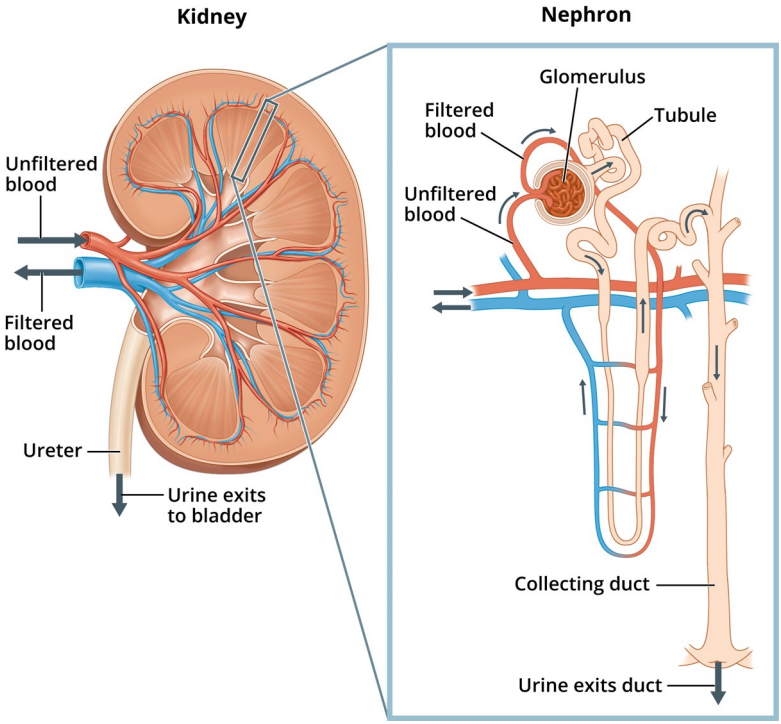

Fig. 1. Image of a close-up nephron and its place in the kidney. Labels on the kidney cross-section show where unfiltered blood enters, filtered blood leaves, and urine exits. On the nephron, the glomerulus, tubule, and collecting duct are labeled along with where unfiltered blood enters, filtered blood exits, and urine exits. Image credit: National Institute of Diabetes and Digestive and Kidney Diseases, National Institutes of Health.

by different compartments. Conservation of volume in the cellular and paracellular compartments (denoted by C and P respectively) is given by:

$$J^i_{v,LC} + J^i_{v,BC} + J^i_{v,PC} = 0 \tag{1}$$

$$J^i_{v,LP} + J^i_{v,BP} + J^i_{v,CP} = 0 \tag{2}$$

where L and B denote the lumen and blood, respectively.

For a given non-reacting solute k (*i.e.*, k =Na^+, K^+, Cl^-, CO_2, urea, or glucose), conservation of mass in the paracellular and cellular space is given by:

$$J^i_{k,LC} + J^i_{k,BC} + J^i_{k,PC} = 0 \tag{3}$$

$$J^i_{k,LP} + J^i_{k,BP} + J^i_{k,CP} = 0 \tag{4}$$

respectively, where $J^i_{k,ab}$ denotes the transmembrane flux of solute k from compartment a to compartment b. Figure 2 shows a schematic of the model compartments.

For reacting solutes, conservation is imposed on the total buffers, so that in the cellular and paracellular compartments (m=C or P) we have:

$$\hat{J}^i_{CO_2,m} + \hat{J}^i_{HCO_3^-,m} + \hat{J}^i_{H_2CO_3,m} = 0 \tag{5}$$

$$\hat{J}^i_{A,m} + \hat{J}^i_{B,m} = 0 \tag{6}$$

where $\hat{J}^i_{k,m}$ is the total flux of solute k into compartment m, so that in particular we have: $\hat{J}^i_{k,C} \equiv J^i_{k,LC} + J^i_{k,BC} + J^i_{k,PC}$ and $\hat{J}_{k,P} \equiv J^i_{k,LP} + J^i_{k,BP} + J^i_{k,CP}$, where (A, B) is a buffer pair (A acid, B base) which is one of (HPO_4^{2-}, $H_2PO_4^-$), (NH_3, NH_4^+), or (HCO_2^-, H_2CO_2).

Additionally, conservation is imposed on the protons so that:

$$\sum_{k \in S_H} \hat{J}^i_{k,m} = 0 \tag{7}$$

for S_H = H^+, NH_4^+, $H_2PO_4^-$, H_2CO_3, and H_2CO_2.

Since ions are charged solutes, across a cell membrane there are both internal and external conducting solutions, which gives a potential difference across the membrane. It is assumed that within each compartment there is electroneutrality so that:

$$\sum_k z_k C^i_{k,m} = 0 \tag{8}$$

where z_k is the valence of solute k, $C^i_{k,m}$ is the concentration of solute k in compartment m (m = P or C).

2.2 Membrane transport processes

2.2.1 Volume transport

For a membrane between compartments a and b, for a segment i, volume flux is denoted by $J^i_{v,ab}$ and given by the Kedem-Katchalsky equation for water transport:

$$J^i_{v,ab} = A^i_{ab} L^i_{p,ab} \left(\sigma^i_{ab} \Delta\pi^i_{ab} + \Delta P^i_{ab} \right) \tag{9}$$

where A^i_{ab} denotes the membrane area, $L^i_{p,ab}$ denotes the hydraulic permeability, σ^i_{ab} is the reflection coefficient,

$$\Delta\pi^i_{ab} = RT\Sigma_k \Delta C^i_{k,ab}$$

where $\Sigma_k \Delta C^i_{k,ab}$ is the osmolality difference where $C^i_{a,b}$ denotes the concentration gradient of solute k along membrane a, b, R is the ideal gas constant, T is the thermodynamic temperature, and ΔP^i_{ab} is the hydrostatic pressure gradient.

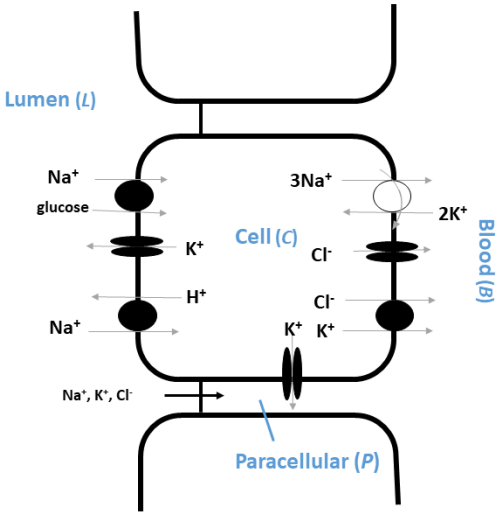

Fig. 2. Schematic diagram of epithelial cells along the nephron. Paracellular transport occurs in the paracellular space. Transcellular transport across the cell membranes.

2.2.2 Solute transport

Unlike transmembrane volume flux ($J^i_{v,ab}$) given in Equation (9), transmembrane solute flux ($J^i_{k,ab}$) depends on electrodiffusion through channels, coupled transport through transporters, and primary active transport across ATP-driven pumps. In general, for a solute k across membrane a, b, solute flux $J^i_{k,ab}$ is given by:

$$J^i_{k,ab} = \left(1 - \sigma^i_{k,ab}\right) \bar{C}^i_{k,ab} J^i_{v,ab} + J^i_{k,ab}(\text{electrodiffusive}) + J^i_{k,ab}(\text{coupled}) + J^i_{k,ab}(\text{ATP-driven}) \tag{10}$$

where the first term represents convective transport, $\sigma^i_{k,ab}$ is the reflection coefficient, and:

$$\bar{C}^i_{k,ab} = \frac{C^i_{k,a} - C^i_{k,b}}{\ln C^i_{k,a} - \ln C^i_{k,b}} \tag{11}$$

is the mean membrane solute concentration where $C^i_{k,a}$ and $C^i_{k,b}$ denote the concentrations of solute k in compartment a and b of segment i, respectively.

The second term in Equation (10), $J^i_{k,ab}(\text{electrodiffusive})$, denotes solute transport via electrodiffusive flux. For ions, electrodiffusive flux is given by the Goldman-Hodgkin-Katz equation:

$$J^i_{k,ab}(\text{electrodiffusive}) = h^i_{k,ab} \zeta^i_{k,ab} \left(\frac{C^i_{k,a} - C^i_{k,b} \exp\left(-\zeta^i_{k,ab}\right)}{1 - \exp\left(-\zeta^i_{k,ab}\right)} \right) \tag{12}$$

where $h^i_{k,ab}$ is the membrane permeability for solute k,

$$\zeta^i_{k,ab} = \frac{z_k F}{RT} \Delta V^i_{ab}$$

where z_k is the solute valence, F is Faraday's constant, R is the ideal gas constant, T is the thermodynamic temperature, and ΔV^i_{ab} denotes the electrical potential difference.

For an uncharged solute, the electrodiffusive flux is given by simple diffusion:

$$J^i_{k,ab}(\text{electrodiffusive}) = h^i_{k,ab} \left(C^i_{k,a} - C^i_{k,b} \right) \tag{13}$$

since transport only depends on the concentration gradient (*i.e.*, not on the electric potential).

The third term in Equation (10), $J^i_{k,ab}(\text{coupled})$, denotes the total coupled transport of a solute k across cotransporters and exchangers. The final term in Equation (10), $J^i_{k,ab}(\text{ATP-driven})$, denotes the total transport via primary active transport (*i.e.*, across ATPases). Transport via cotransporters, exchangers, and primary active transport is described below.

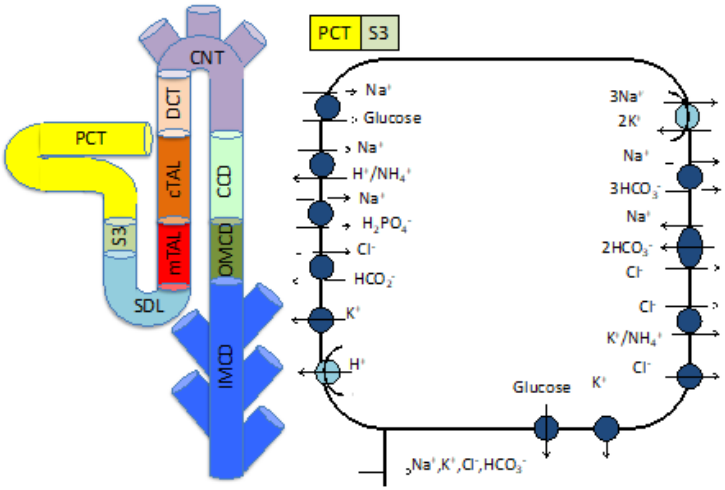

Fig. 3. (Left) A schematic diagram of a nephron, showing its segments in different colors (not to scale). *(Right)* The epithelial transport model corresponding to a proximal tubule cell. Only major Na+ membrane transporters are shown. *E.g.*, on the apical membrane *(left)*, the sodium-hydrogen exchanger is shown (second transporter from top); on the basolateral membrane *(right)*, the Na+/K+-ATPase pump is shown *(first from top)*. PCT: proximal convoluted tubule; SDL: short descending limb; mTAL: medullary thick ascending limb; cTAL: cortical thick ascending limb; DCT: distal convoluted tubule; CNT: connecting tubule; CCD: cortical collecting duct; OMCD: outer-medullary collecting duct; IMCD: inner-medullary collecting duct

2.3 Modeling membrane transporters

Transport via cotransporters, exchangers, and primary active transport are modeled based on existing kinetic models for each transporter. Here we highlight a few key transporters and how they are modeled. More details are provided in Layton and Edwards.[2]

2.3.1 Sodium-hydrogen exchanger

The Na^+/H^+ exchanger isoform 3 (NHE3) is located in the proximal tubule. NHE3 exchanges Na^+ from the lumen with intracellular H^+ or NH_4^+. That is, there is competitive binding of intracellular H^+ and NH_4^+. Indeed, NHE3 plays a major role in both NH_4^+ secretion and Na^+ reabsorption in the proximal tubule. A schematic diagram of a proximal tubule cell is shown in Figure 3. The model for NHE3 transport was originally developed by Weinstein *et al.*[3] and is described below.

Following the same notation and approach as in in Weinstein *et al.*,[3] let A, B, C denote Na^+, H^+, and NH_4^+, respectively, with X denoting an empty NHE3 transporter. Then let a^i and a^e denote the intracellular $[Na^+]$ and extracellular $[Na^+]$, respectively and analogously for $[H^+]$ and $[NH_4^+]$ (*i.e.*, using lower case b and c). Similarly, let x^i, x^e denote empty transporter density on the internal and external face of the membrane, respectively, and ax denotes the complex of Na^+ with a transporter, so that we can let:

$$K_a = \frac{a^i x^i}{(ax)^i} = \frac{a^e x^e}{(ax)^e} \tag{14}$$

where K_a is an equilibrium constant for Na^+. Similarly letting b denote the $[H^+]$ and c denote $[NH_4^+]$ we have:

$$K_b = \frac{b^i x^i}{(bx)^i} = \frac{b^e x^e}{(bx)^e}, \qquad K_c = \frac{c^i x^i}{(cx)^i} = \frac{c^e x^e}{(cx)^e} \tag{15}$$

where K_b and K_c are equilibrium constants for H^+ and NH_4^+, respectively.

The total amount of carrier (denoted by x_{T}) is assumed to be conserved so that:

$$x^i + (ax)^i + (bx)^i + (cx)^i + x^e + (ax)^e + (bx)^e + (cx)^e = x_T \tag{16}$$

and that the net flux is zero so that:

$$T_a(ax)^i + T_b(bx)^i + T_c(cx)^i = T_a(ax)^e + T_b(bx)^e + T_c(cx)^e, \tag{17}$$

where T_k is the transport rate of solute k. Next, let:

$$\alpha \equiv \frac{a}{K_a}, \qquad \beta \equiv \frac{b}{K_b}, \qquad \gamma \equiv \frac{c}{K_c} \tag{18}$$

be non-dimensionalized concentrations. Note that by Equation (14) we have that:

$$(ax)^i = \frac{a^i}{K_a} x^i = \alpha^i x^i \tag{19}$$

and in the same way $(bx)^i = \beta^i x^i$ and $(cx)^i = \gamma^i x^i$. Also, the same can be done for the extracellular concentrations. Then plugging this into Equation (16) we have that:

$$x^i \left(1 + \alpha^i + \beta^i + \gamma^i\right) + x^e \left(1 + \alpha^e + \beta^e + \gamma^e\right) = x_T. \tag{20}$$

Similarly, Equation(17) can then be rewritten as:

$$-x^i \left(T_a\alpha^i + T_b\beta^i + T_c\gamma^i\right) + x^e \left(T_a\alpha^e + T_b\beta^e + T_c\gamma^e\right) = 0. \tag{21}$$

Thus, Equation (20) and Equation (21) give a 2×2 system of equations to solve for x^i and x^e:

$$\begin{pmatrix} 1 + \alpha^i + \beta^i + \gamma^i & 1 + \alpha^e + \beta^e + \gamma^e \\ -\left(T_a\alpha^i + T_b\beta^i + T_c\gamma^i\right) & T_a\alpha^e + T_b\beta^e + T_c\gamma^e \end{pmatrix} \begin{pmatrix} x^i \\ x^e \end{pmatrix} = \begin{pmatrix} x_T \\ 0 \end{pmatrix}$$

by using Cramer's rule.

Let Σ denote the determinant of the matrix so that:

$$\Sigma = (1+\alpha^i+\beta^i+\gamma^i)(T_a\alpha^e+T_b\beta^e+T_c\gamma^e)+(T_a\alpha^i+T_b\beta^i+T_c\gamma^i)(1+\alpha^e+\beta^e+\gamma^e) \tag{22}$$

so that:

$$x^i = x_T(T_a\alpha^e + T_b\beta^e + T_c\gamma^e)/\Sigma \tag{23}$$

$$x^e = x_T(T_a\alpha^i + T_b\beta^i + T_c\gamma^i)/\Sigma. \tag{24}$$

The flux of Na^+, H^+, and NH_4^+ across the NHE3 can now be computed.

Let J_a denote the outward flux of Na^+ across the NHE3 so that:

$$J_a = T_a(ax)^i - T_a(ax)^e \tag{25}$$

which using Equation (19) we get that:

$$J_a = T_a\left(\alpha^i x^i - \alpha^e x^i - \alpha^e x^e\right). \tag{26}$$

Then substitute Equations (23) and (24) into Equation (26) and similarly for the NH_4^+ and H^+ to get:

$$J_a = \frac{x_T T_a}{\Sigma}\left[T_b\left(\alpha^i\beta^e - \alpha^e\beta^i\right) + T_c\left(\alpha^i\gamma^e - \alpha^e\gamma^i\right)\right] \tag{27}$$

$$J_b = \frac{x_T T_b}{\Sigma}\left[T_a\left(\beta^i\alpha^e - \beta^e\alpha^i\right) + T_c\left(\beta^i\gamma^e - \beta^e\gamma^i\right)\right] \tag{28}$$

$$J_c = \frac{x_T T_c}{\Sigma}\left[T_a\left(\gamma^i\alpha^e - \gamma^e\alpha^i\right) + T_b\left(\gamma^i\beta^e - \gamma^e\beta^i\right)\right] \tag{29}$$

Hence, using the internal and external concentrations of Na^+, H^+, and NH_4^+, translocation rates, and carrier amount can be used to compute the fluxes across the NHE3 antiporter.

Weinstein *et al.* fit the model parameters to experimental kinetics data since these values, such as the translocation rate, cannot be measured directly.[3]. Some assumptions were also made, specifically the translocation rates are fixed and the binding affinities for both internal and external are taken to be equal. The NHE3 model is a type of model that has been extended to capture the transport of other exchangers and transporters, including the Na^+-K^+-$2Cl^-$ and K^+-Cl^- cotransporters.[2]

2.3.2 Na^+-K^+-ATPase pump

The Na^+-K^+-ATPase pump is located on the basolateral side of every cell along the nephron. Na^+-K^+-ATPase is an active transporter and moves 3 Na^+ ions out of the cell in exchange for 2 K^+ ions moving into the cell. Note that intracellular K^+ concentrations are high and intracellular Na^+ concentrations are relatively low, while the opposite is true in the respective extracellular concentrations. The Na^+-K^+-ATPase pump plays a key role in maintaining this concentration gradient. This gradient is important for regulating cell volume as well as maintaining the resting potential. Here we describe how the Na^+-K^+-ATPase pump is modeled in epithelial cell models using the approach described in Layton and Edwards.[2]

The flux of Na^+ and K^+ across Na^+-K^+-ATPase can be determined by considering this transport mechanism as a binding of each of the ions to an enzyme independently. First, assume that the binding of one Na^+ ion (intracellular) to a free enzyme (denoted by E) form a Na^+-E complex (denoted by NaE) in a first-order, reversible reaction so that:

$$\mathrm{Na^+ + E} \underset{k_-}{\overset{k_+}{\rightleftharpoons}} \mathrm{NaE}$$

so that the rate of formation of the complex NaE is given by:

$$\frac{dC_{NaE}}{dt} = k_+ C_{Na} C_E - k_- C_{NaE} \tag{30}$$

where C_{NaE}, C_E, C_{Na} denote the concentration of NaE, E, and intracellular Na^+, respectively. Let $C_E^{\text{total}} = C_E + C_{NaE}$ so that then we can rewrite Equation (30) as:

$$\frac{dC_{NaE}}{dt} = k_+ C_{Na} C_E^{\text{total}} - \left(k_+ C_{Na} + k_-\right) C_{NaE} \tag{31}$$

which we can then set to steady state to get that:

$$C_{NaE} = \frac{k_+ C_{Na} C_E^{\text{total}}}{k_+ C_{Na} + k_-} = \frac{C_{Na} C_E^{\text{total}}}{C_{Na} + K_{Na}} \tag{32}$$

where $K_{Na} = k_-/k_+$ is the dissociation constant for the NaE complex. This means that the probability of having one Na^+ ion bind to one Na^+-K^+-ATPase pump is proportional to:

$$\frac{C_{Na}}{C_{Na} + K_{Na}}.$$

Letting p_{Na} denote this probability, if the binding of the Na^+ to the three Na^+-K^+-ATPase binding sites is assumed to be independent (*i.e.*, no cooperativity), then the probability of all three sites having Na^+ ions bound to them is p_{Na}^3. In the same way, letting p_K denote the probability of having an extracellular K^+ ion bound to a K^+ binding site, the probability of both K^+ binding sites having a K^+ bound to them is p_K^2 where p_K is proportional to:

$$\frac{C_K}{C_K + K_K}$$

where C_K is the concentration of external K^+ and K_K denotes the dissociation of the K^+ and free enzyme complex. As such, we can determine the flux of Na^+ ions across the Na^+-K^+-ATPase pump as:

$$J_{Na}^{NaK} = J_{Na}^{NaK,max} \left[\frac{C_{Na}}{C_{Na} + K_{Na}}\right]^3 \left[\frac{C_K}{C_K + K_K}\right]^2 \tag{33}$$

where $J_{Na}^{NaK,max}$ is the maximum efflux of Na^+ ions at steady state, which is a parameter. Then note that for every 3 Na^+ ions pumped, there are 2 K^+ ions pumped across the Na^+-K^+-ATPase pump so that we can compute the flux of K^+ across the Na^+-K^+-ATPase pump as:

$$J_K^{NaK} = -(2/3) J_{Na}^{NaK}. \tag{34}$$

The parameters for Equation (33) and Equation (34) have been determined in previous model development for each of the nephron segments.[2,4]

3. Regulation and adaptation of membrane transport

3.1 Volume-regulated anion channels

Unlike plant cells, animal cells lack a rigid cell wall and most have water-permeable membranes. As such, a transmembrane osmolality gradient would drive water movement across the cell membrane, resulting in changes in cell volume. To avoid large fluctuations in cell volume that can impair the cell's structural integrity and function, animal cells rely on regulatory mechanisms to adjust the rate of solute transport across cell membranes and/or cellular metabolism. Such mechanisms include the activation of transport pathways, including channels and coupled transporters, that allow inorganic osmolytes to regulate water flow.[5] For example, stimulation of K^+ and Cl^- channels, as well as K^+-Cl^-, and other electroneutral cotransporters, leads to a loss of KCl and other solutes, thereby reducing cell swelling. In contrast, activating Na^+-K^+-$2Cl^-$ and/or Na^+-Cl^- cotransporters, Na^+/H^+, and Cl^-/HCO_3^- exhcangers results in a gain of NaCl and other solutes to counteract cell shrinkage.[6]

To simulate cell volume regulation, the volume of the cellular and paracellular compartments are allowed to vary:[7]

$$\frac{d}{dt}V_C(t) = J_{v,LC}(t) + J_{v,BC}(t) + J_{v,PC}(t) \tag{35}$$

$$\frac{d}{dt}V_P(t) = J_{v,LP}(t) + J_{v,BP}(t) + J_{v,CP}(t). \tag{36}$$

One mechanism by which the renal proximal tubule cells regulate volume is by adjusting the membrane expression of basolateral Cl^- channels. To represent this mechanism, we define target Cl^- channel expression level, denoted by $\bar{x}_{\mathrm{Cl}}$, taken to be increasing functions of cell volume V. Specifically, we assume that:

$$\bar{x}_{\mathrm{Cl}}(t) = x^0_{\mathrm{Cl}}\left(1 + (G-1) \times \left(\frac{\Delta V(t)}{\mu}\right)^2\right). \tag{37}$$

In the above expression, the superscript "0" denotes baseline values, and ΔV denotes the fractional deviation in cell volume, given by $\Delta V = V(t)/V0 - 1$. G and μ are determined from experimental data. The rate of change in the membrane expression of Cl^- channels is then given by:

$$\frac{d}{dt}x_{\mathrm{Cl}}(t) = \frac{1}{\tau}\left(\bar{x}_{\mathrm{Cl}}(t) - x_{\mathrm{Cl}}(t)\right) \tag{38}$$

where τ denotes the time constant.

Edwards and Layton incorporated cell volume regulatory mechanisms into a computational model of the proximal convoluted tubule cell, and examined the model cell's response to a hypoosmotic challenge, in which the bath osmolality was lowered by 80 mosm/(kg H2O).[7] In the absence of regulatory volume decrease mechanisms, cell volume increased by 14%, lowering the intracellular concentrations of most solutes. In contrast, activation of volume regulatory mechanisms attenuated cell swelling, with a steady-state volume that is 5% above baseline, one-third of the predicted expansion without regulation. These results are in agreement with the observations of Völkl and Lang,[8] who observed a 6% increase in cell volume in perfused mouse proximal straight tubules after a 80 mosm/(kg H2O) decrease in bath solution osmolality. Similarly, in cultured mouse proximal convoluted tubule cells, cell volume returned to 105% of its original value when the osmolality of the surrounding solution was reduced by 100 mosm/(kg H2O).[9]

In the eyes, volume-regulated anion channels have been shown to modulate the volume of trabecular meshwork cells and, in turn, the aqueous humor outflow.[10,11] The balance between the secretion and the drainage of aqueous humor determines the intraocular pressure, which is the major causal risk factor for glaucoma.

3.2 Sexual dimorphism in membrane transporter patterns

Physiological differences between males and females are by no means limited to the reproductive system. Sex differences in renal function and blood pressure have been

widely described across many species.[12] It is well established that young males have a higher blood pressure and a higher prevalence of hypertension compared with age-matched females in many mammalian and avian species. In humans[13] and in genetic models of hypertension, such as spontaneously hypertensive rats and Dahl salt-sensitive rats,[14] males develop an earlier and more severe hypertension than females. To date, the mechanisms underlying male-female differences in blood pressure control remain poorly understood. In the past few years, an explosion of data has emerged concerning sex differences in nitric oxide (NO),[15] the renin-angiotensin aldosterone system (RAAS),[16,17] inflammation,[18,19] and in kidney function.[20,21]

Exciting findings reported by Veiras *et al.* have highlighted the fact that the kidney of a female rat is not simply a smaller version of a male kidney.[22] Rather, male and female kidneys exhibit dimorphic patterns of transporter expression and salt handling,[22] the implications of which could be profound in terms of renal function. Li *et al.* incorporated those findings into a computational model of solute and water transport along the proximal convoluted tubule of the rat kidney and applied the resulting sex-specific models to investigate the functional implication of sexual dimorphism in transporter patterns along that segment.[23] The models account for the sex differences in expression levels of the apical and basolateral transporters, in single-nephron glomerular filtration rate (GFR), and in tubular dimensions. Model simulations indicate that the lower fractional volume reabsorption in the female can be attributed to their smaller transport area and lower aquaporin-1 expression level. Additionally, model results suggest that the higher sodium glucose cotransporter 2 (SGLT2) expression in the female may compensate for its lower transport area to achieve a similar hyperglycemic tolerance as male.[24] Later studies extended this model to develop sex-specific models of a full superficial nephron in the rat kidney,[25] full rat kidney,[26] and human kidneys.[27,28] Few studies in the literature have thoroughly investigated the basic physiological differences in renal structure and function, yet these studies underscore the importance of improving our understanding of the basic physiological characteristics of the female kidney.

3.3 Adaptation of membrane transport in physiological and pathophysiological conditions

3.3.1 Pregnancy

Pregnancy induces major changes in the kidneys to sufficiently supply the demands of the rapidly developing fetus and placenta. Specifically, the maternal body must support a plasma volume expansion of approximately 40–50% as well as retain electrolytes.[29,30] These changes are essential for sufficient perfusion of the fetus and placenta in order to support a healthy pregnancy. These adaptations are relevant to the kidneys because of their role in electrolyte and volume homeostasis. In the kidneys, there are adaptations in transporter expression,[30] hemodynamics,[29] and morphology.[31] In particular, the GFR is increased by approximately 50%, the kidney volume increases, which includes increased length of the proximal tubule, and many

key transporters have altered activity and expression levels.[29–31] These changes are complex and multifactorial.

Stadt and Layton developed computational models to investigate how pregnancy-induced changes effect Na^+ and K^+ reabsorption in a superficial rat nephron.[32] Specifically, simulations and subsequent analysis were used to predict that morphological renal adaptations as well as increased NHE3 and epithelial Na^+ channel activity were key in maintaining increased Na^+ reabsorption through pregnancy. Additionally, they found that decreased K^+ secretory channels in the distal segments along with increased distal segment transporter H^+-K^+-ATPase activity are essential to prevent excess K^+ loss through pregnancy.

Major physiological changes happen in nearly all tissues and organs in the maternal body.[33,34] Indeed, pregnancy also affects the eyes.[35,36] Some of these changes include changes in corneal thickness and curvature as well as increases in sensation that may cause sensitivity to contact lenses. These changes are likely due to altered fluid homeostasis during pregnancy as well as the impacts of hormones such as estrogen and progesterone. Additionally, it has been shown that disorders of the eye such as glaucoma or diabetic retinopathy can be worsened due to pregnancy-induced changes in the eyes.[35] The altered physiological state of pregnancy may benefit from investigations through computational modeling.

3.3.2 Diabetes

Diabetes induces renal hypertrophy, hyperfiltration (with GFR elevated by 50%), and alterations in the expression of the glucose transporters, sodium-glucose cotransporters 2 and 1 (SGLT2 and SGLT1), and glucose transporters 2 and 1 (GLUT2 and GLUT1). In addition, diabetes has been found to induce changes in the expression of other sodium transporters along the rat nephron (*i.e.*, the sodium-hydrogen exchanger NHE3, the epithelial sodium channel ENaC, and the Na^+-K^+-ATPase pump), as well as that of aquaporin water channels. The quantitative changes differ significantly between studies, and very early changes (*i.e.*, a few days after the administration of streptozotocin) appear stronger, possibly as a response to osmotic diuresis and some volume depletion.

In a modeling study,[37] Layton *et al.* investigated how diabetes and SGLT2 inhibition affect the reabsorption of Na^+ and sodium transport-dependent oxygen consumption along the nephrons. Diabetes increases the reabsorption of Na^+ and glucose via the sodium-glucose cotransporter SGLT2 in the early proximal tubule of the renal cortex. Relative to the normal rat kidney, the model predicts a 50% increase in total Na+ transport. That increase, which is comparable to *in vivo* data of O'Neill *et al.*,[38] is attributable, in large part, to the filtration rate increase.

The breakdown of the blood-retinal barrier in diabetic retinopathy is well studied. Less well studied is the effect of diabetes on the transepithelial transport across the retinal pigment epithelium. Not only do tight junctions disassemble in the latter stages of the disease, but subtler effects on barrier function may contribute signifi-

cantly to the pathophysiology. Hyperglycemia can have detrimental effects on retinal pigment epithelium by decreasing the activity of Na^+-K^+-ATPase, and consequently, the electrochemical gradients that drive transcellular transport. Disruption of the electrochemical gradients would compromise the supply of nutrients to the retina and hinder the removal of metabolic waste. It would also disrupt the ionic milieu of the subretinal space that is essential for neuronal function. Besides tight junction proteins, diabetes may also alter glucose transporters and aquaporin proteins.[39]

4. Discussion

The nephrons are nothing short of amazing. Together, they reabsorb on average of 180 L of water every day. The most challenging aspect of their task is not the heavy load, but the need to simultaneously achieve a number of goals: electrolyte homeostasis, body fluid homeostasis, acid-base balance, and excretion of toxic waste. As such, the nephrons consist of several populations of epithelial cells, each "fitted" with a unique set of membrane transporters and channels, to handle tubular fluid with differing composition. Luminal fluid at the beginning of the nephron has a composition similar to blood plasma, but by the time that fluid reaches the end of the collecting duct system, it has been transformed into urine. With this complex setup, a healthy kidney can transport just the right amount of water and solutes to achieve the homeostatic targets, often under constantly varying conditions, impacted by hydration status and food intake.

Substantial effort, both experimental and theoretical, has been invested to unravel kidney function under a host of physiological and pathophysiological conditions. *How do mammals produce a urine that is substantially more concentrated than urine?*[40–42] The kidney is among the organs with the highest metabolic demand, given its size. Indeed, for the kidneys to function properly, GFR must be maintained without a narrow window. *How do the kidneys regulate their blood flow, and thus, oxygen supply?* The answer is that this regulation is achieved via several interacting feedback mechanisms.[43–45] *How does kidney function differ between males and females?*[25–27] *How is kidney function altered under pathophysiological conditions*[46–48] *or in pregnancy?*[32] As discussed in this review, computational models that simulate solute and water transport have been built to answer these questions.

In addition to holding a key to some of the aforementioned questions regarding kidney function, membrane transport also plays a key role in mediating essential eye function, including the production of aqueous humor and transmembrane pressure balance. Indeed, computational models have been developed to address these questions.[49–51] Given the similarities between the transport processes in these organs, cross-fertilization of the modeling effort will likely benefit both communities.

Declarations

Ethics approval and consent to participate

Not required.

Competing interests

None to declare.

Funding

This study is partially supported by the Canada 150 Research Chairs Program, the Natural Sciences and Engineering Research Council of Canada (NSERC Discovery award: RGPIN-2019-03916).

Acknowledgements

None to declare.

References

1. Eaton DC, Pooler J, Vander AJ. Vander's renal physiology. en. 7th. OCLC: 340936292. New York: McGraw-Hill Medical, 2009; ISBN: 978-0-07-161304-0. Available from: http://www.accessmedicine.com/resourceTOC.aspx?resourceID=57, visited on 11/13/2021,
2. Layton AT, Edwards A. Mathematical Modeling in Renal Physiology. eng. 1st ed. 2014. Lecture Notes on Mathematical Modelling in the Life Sciences. Berlin, Heidelberg: Springer Berlin Heidelberg, 2014; ISBN: 978-3-642-27367-4. doi: 10.1007/978-3-642-27367-4.
3. Weinstein AM. A kinetically defined Na+/H+ antiporter within a mathematical model of the rat proximal tubule. en. Journal of General Physiology, May 1995;105(5): 617–641. ISSN: 0022-1295, 1540-7748. Available from: https://rupress.org/jgp/article/105/5/617/26432/A-kinetically-defined-NaH-antiporter-within-a, visited on 11/22/2021, doi: 10.1085/jgp.105.5.617.
4. Layton AT, Vallon V, Edwards A. A computational model for simulating solute transport and oxygen consumption along the nephrons. eng. American journal of physiology. Renal physiology, 2016;311(6): Place: United States Publisher: American Physiological Society, F1378–F1390. ISSN: 1931-857X. doi: 10.1152/ajprenal.00293.2016.
5. Okada Y. Ion channels and transporters involved in cell volume regulation and sensor mechanisms. Cell biochemistry and biophysics, 2004;41(2): 233–258.
6. Hoffmann EK, Dunham PB. Membrane mechanisms and intracellular signalling in cell volume regulation. International review of cytology, 1995;161, 173–262.
7. Edwards A, Layton AT. Cell volume regulation in the proximal tubule of rat kidney. Bulletin of mathematical biology, 2017;79(11): 2512–2533.
8. Völkl H, Lang F. Effect of potassium on cell volume regulation in renal straight proximal tubules. The Journal of membrane biology, 1990;117(2): 113–122.
9. Barriere H, Rubera I, Belfodil R, Tauc M, Tonnerieux N, Poujeol C, et al. Swelling-activated chloride and potassium conductance in primary cultures of mouse proximal tubules. Implication of KCNE1 protein. The Journal of membrane biology, 2003;193(3): 153–170.

10. Mitchell CH, Fleischhauer JC, Stamer WD, Peterson-Yantorno K, Civan MM. Human trabecular meshwork cell volume regulation. American Journal of Physiology-Cell Physiology, 2002;283(1): C315–C326.
11. Soto D, Comes N, Ferrer E, Morales M, Escalada A, Palés J, et al. Modulation of aqueous humor outflow by ionic mechanisms involved in trabecular meshwork cell volume regulation. Investigative ophthalmology & visual science, 2004;45(10): 3650–3661.
12. Sandberg K, Ji H. Sex differences in primary hypertension. Biology of sex differences, 2012;3(1): 1–21.
13. Wiinberg N, Høegholm A, Christensen HR, Bang LE, Mikkelsen KL, Nielsen PE, et al. 24-h ambulatory blood pressure in 352 normal Danish subjects, related to age and gender. American journal of hypertension, 1995;8(10): 978–986.
14. Ouchi Y, Share L, Crofton JT, Iitake K, Brooks DP. Sex difference in the development of deoxycorticosterone-salt hypertension in the rat. Hypertension, 1987;9(2): 172–177.
15. Chen Y, Sullivan JC, Edwards A, Layton AT. Sex-specific computational models of the spontaneously hypertensive rat kidneys: factors affecting nitric oxide bioavailability. American Journal of Physiology-Renal Physiology, 2017;313(2): F174–F183.
16. Hilliard LM, Sampson AK, Brown RD, Denton KM. The "his and hers" of the renin-angiotensin system. Current hypertension reports, 2013;15(1): 71–79.
17. Leete J, Gurley S, Layton AT. Modeling sex differences in the renin angiotensin system and the efficacy of antihypertensive therapies. Computers & chemical engineering, 2018;112, 253–264.
18. Pollow DP, Uhrlaub J, Romero-Aleshire MJ, Sandberg K, Nikolich-Zugich J, Brooks HL, et al. Sex differences in T-lymphocyte tissue infiltration and development of angiotensin II hypertension. Hypertension, 2014;64(2): 384–390.
19. Tipton AJ, Baban B, Sullivan JC. Female spontaneously hypertensive rats have a compensatory increase in renal regulatory T cells in response to elevations in blood pressure. Hypertension, 2014;64(3): 557–564.
20. Munger K, Baylis C. Sex differences in renal hemodynamics in rats. American Journal of Physiology-Renal Physiology, 1988;254(2): F223–F231.
21. Sabolić I, Asif AR, Budach WE, Wanke C, Bahn A, Burckhardt G. Gender differences in kidney function. Pflügers Archiv-European Journal of Physiology, 2007;455(3): 397–429.
22. Veiras LC, Girardi AC, Curry J, Pei L, Ralph DL, Tran A, et al. Sexual dimorphic pattern of renal transporters and electrolyte homeostasis. Journal of the American Society of Nephrology, 2017;28(12): 3504–3517.
23. Li Q, McDonough AA, Layton HE, Layton AT. Functional implications of sexual dimorphism of transporter patterns along the rat proximal tubule: modeling and analysis. American Journal of Physiology-Renal Physiology, 2018;315(3): F692–F700.
24. Sabolić I, Vrhovac I, Eror DB, Gerasimova M, Rose M, Breljak D, et al. Expression of Na+-D-glucose cotransporter SGLT2 in rodents is kidney-specific and exhibits sex and species differences. American Journal of Physiology-Cell Physiology, 2012;302(8): C1174–C1188.
25. Hu R, McDonough AA, Layton AT. Functional implications of the sex differences in transporter abundance along the rat nephron: modeling and analysis. eng. American journal of physiology. Renal physiology. Sex and Gender in Renal Health and Function, 2019;317(6): Place: United States Publisher: American Physiological Society, F1462–F1474. ISSN: 1931-857X. doi: 10.1152/ajprenal.00352.2019.
26. Hu R, McDonough AA, Layton AT. Sex differences in solute transport along the nephrons: effects of Na+ transport inhibition. eng. American journal of physiology. Renal physiology, 2020;319(3): F487–F505. ISSN: 1931-857X. doi: 10.1152/ajprenal.00240.2020.
27. Hu R, McDonough AA, Layton AT. Sex differences in solute and water handling in the human kidney: Modeling and functional implications. en. iScience, June 2021;24(6): 102667. ISSN: 2589-0042. Available from: https://www.sciencedirect.com/science/article/pii/S2589004221006350, visited on 06/21/2021, doi: 10.1016/j.isci.2021.102667.

28. Swapnasrita S, Carlier A, Layton AT. Sex-Specific Computational Models of Kidney Function in Patients With Diabetes. Frontiers in Physiology, 2022;13. ISSN: 1664-042X. Available from: https://www.frontiersin.org/article/10.3389/fphys.2022.741121, visited on 03/04/2022,
29. West CA, Sasser JM, Baylis C. The enigma of continual plasma volume expansion in pregnancy: critical role of the renin-angiotensin-aldosterone system. American Journal of Physiology-Renal Physiology, Oct. 2016;311(6): Publisher: American Physiological Society, F1125–F1134. ISSN: 1931-857X. Available from: http://journals.physiology.org/doi/full/10.1152/ajprenal.00129.2016, visited on 05/06/2021, doi: 10.1152/ajprenal.00129.2016.
30. Souza AMA de, West CA. Adaptive remodeling of renal Na+ and K+ transport during pregnancy. en-US. Current Opinion in Nephrology and Hypertension, Sept. 2018;27(5): 379–383. ISSN: 1062-4821. Available from: https://journals.lww.com/co-nephrolhypertens/Abstract/2018/09000/Adaptive_remodeling_of_renal_Na__and_K__transport.10.aspx, visited on 05/06/2021, doi: 10.1097/MNH.0000000000000441.
31. Atherton J, Pirie SC. The effect of pregnancy on glomerular filtration rate and salt and water reabsorption in the rat. Journal of Physiology, Jan. 1981;319, 153–164.
32. Stadt MM, Layton AT. Adaptive changes in single-nephron GFR, tubular morphology, and transport in a pregnant rat nephron: modeling and analysis. American Journal of Physiology-Renal Physiology, Feb. 2022;322(2): Publisher: American Physiological Society, F121–F137. ISSN: 1931-857X. Available from: https://journals.physiology.org/doi/full/10.1152/ajprenal.00264.2021, visited on 01/21/2022, doi: 10.1152/ajprenal.00264.2021.
33. Napso T, Yong HEJ, Lopez-Tello J, Sferruzzi-Perri AN. The Role of Placental Hormones in Mediating Maternal Adaptations to Support Pregnancy and Lactation. en. Frontiers in Physiology, Aug. 2018;9, 1091. ISSN: 1664-042X. Available from: https://www.frontiersin.org/article/10.3389/fphys.2018.01091/full, visited on 06/10/2021, doi: 10.3389/fphys.2018.01091.
34. Abo S, Smith D, Stadt M, Layton A. Modelling Female Physiology from Head to Toe: Impact of Sex Hormones, Menstrual Cycle, and Pregnancy. en. Journal of Theoretical Biology, Feb. 2022; 111074. ISSN: 0022-5193. Available from: https://www.sciencedirect.com/science/article/pii/S0022519322000728, visited on 02/26/2022, doi: 10.1016/j.jtbi.2022.111074.
35. Khong EWC, Chan HHL, Watson SL, Lim LL. Pregnancy and the eye. en-US. Current Opinion in Ophthalmology, Nov. 2021;32(6): 527–535. ISSN: 1040-8738. Available from: https://journals.lww.com/co-ophthalmology/Fulltext/2021/11000/Pregnancy_and_the_eye.6.aspx, visited on 03/02/2022, doi: 10.1097/ICU.0000000000000778.
36. Chawla S, Chaudhary T, Aggarwal S, Maiti GD, Jaiswal K, Yadav J. Ophthalmic considerations in pregnancy. en. Medical Journal Armed Forces India, July 2013;69(3): 278–284. ISSN: 0377-1237. Available from: https://www.sciencedirect.com/science/article/pii/S0377123713000440, visited on 03/03/2022, doi: 10.1016/j.mjafi.2013.03.006.
37. Layton AT, Vallon V, Edwards A. Modeling oxygen consumption in the proximal tubule: effects of NHE and SGLT2 inhibition. American Journal of Physiology-Renal Physiology, 2015;308(12): F1343–F1357.
38. O'Neill J, Fasching A, Pihl L, Patinha D, Franzén S, Palm F. Acute SGLT inhibition normalizes O2 tension in the renal cortex but causes hypoxia in the renal medulla in anaesthetized control and diabetic rats. American journal of physiology-renal physiology, 2015;309(3): F227–F234.
39. Xia T, Rizzolo LJ. Effects of diabetic retinopathy on the barrier functions of the retinal pigment epithelium. Vision research, 2017;139, 72–81.
40. Layton AT. A mathematical model of the urine concentrating mechanism in the rat renal medulla. II. Functional implications of three-dimensional architecture. American Journal of Physiology-Renal Physiology, 2011;300(2): F372–F384.
41. Layton AT. A mathematical model of the urine concentrating mechanism in the rat renal medulla. I. Formulation and base-case results. American Journal of Physiology-Renal Physiology, 2011;300(2): F356–F371.
42. Layton AT, Layton HE. A region-based model framework for the rat urine concentrating mechanism. Bulletin of mathematical biology, 2003;65(5): 859–901.

43. Chen J, Sgouralis I, Moore LC, Layton HE, Layton AT. A mathematical model of the myogenic response to systolic pressure in the afferent arteriole. American Journal of Physiology-Renal Physiology, 2011;300(3): F669–F681.
44. Layton AT. Feedback-mediated dynamics in a model of a compliant thick ascending limb. Mathematical biosciences, 2010;228(2): 185–194.
45. Layton AT, Moore LC, Layton HE. Multistable dynamics mediated by tubuloglomerular feedback in a model of coupled nephrons. Bulletin of mathematical biology, 2009;71(3): 515–555.
46. Layton AT, Edwards A, Vallon V. Adaptive changes in GFR, tubular morphology, and transport in subtotal nephrectomized kidneys: modeling and analysis. American Journal of Physiology-Renal Physiology, 2017;313(2): F199–F209.
47. Hu R, Layton A. A computational model of kidney function in a patient with diabetes. International journal of molecular sciences, 2021;22(11): 5819.
48. Layton AT, Vallon V. SGLT2 inhibition in a kidney with reduced nephron number: modeling and analysis of solute transport and metabolism. American Journal of Physiology-Renal Physiology, 2018;314(5): F969–F984.
49. Avtar R, Srivastava R, Nigam D. A mathematical model for solute coupled water transport in the production of aqueous humor. Applied mathematical modelling, 2008;32(7): 1350–1369.
50. Cheng X, Pinsky PM. The balance of fluid and osmotic pressures across active biological membranes with application to the corneal endothelium. PloS one, 2015;10(12): e0145422.
51. Sacco R, Guidoboni G, Jerome JW, Bonifazi G, Marazzi NM, Verticchio Vercellin AC, et al. A theoretical approach for the electrochemical characterization of ciliary epithelium. Life, 2020;10(2): 8.